Research Square

Preprints are preliminary reports that have not undergone peer review.
They should not be considered conclusive, used to inform clinical practice,
or referenced by the media as validated information.

Industrial Effluent Contaminant Plumes Mapping Using Integrated Geophysical and Hydrochemistry Techniques in Ugbolu, Southern Nigeria

John Elvis. Ighodalo

Ighodalo.elvis@uniben.edu

University of Benin

Ikere Povwe Joy

Federal University of Medical and Health Sciences

Alexander Ogbamikhumi

University of Benin

Research Article

Keywords: Electrical Resistivity Tomography, Vertical Electrical Sounding, Groundwater Contamination, Cassava Effluent, Hydrochemistry, Water Quality Index

Posted Date: November 17th, 2026

DOI: https://doi.org/10.21203/rs.3.rs-11450444/v1

License: This work is licensed under a Creative Commons Attribution 4.0 International License.
Read Full License

Additional Declarations: No competing interests reported.

Industrial Effluent Contaminant Plumes Mapping Using Integrated Geophysical and Hydrochemistry Techniques in Ugbolu, Southern Nigeria

Ighodalo John Elvis.[1], Ikere Povwe Joy[2],Alexander Ogbamikhumi, [3]

[1]*Department of Physics, University of Benin, Benin City, Edo State, Nigeria.*
[2]*Federal University of Medical and Health Sciences, Kwale, Delta State, Nigeria.*
[3]*Department of Geology, University of Benin, Benin City, Edo State, Nigeria.*
Corresponding Author's Email: Ighodalo.elvis@uniben.edu

Abstract

The study assesses the risk to shallow groundwater systems at Ugbolu, southern Nigeria, arising from the discharge of effluents from industrial cassava-processing activities. The present study combines two-dimensional electrical resistivity tomography (2D ERT), quasi-three-dimensional resistivity visualisation, Vertical Electrical Sounding (VES), hydrochemical analysis, Water Quality Index (WQI), and hydrochemical facies modelling to identify the conductive sub-surface anomalies and evaluate the groundwater quality in the aquifer of the Benin Formation. Ten ERT profiles, ten VES stations and groundwater samples from five strategically located hand-dug wells have been collected to define the spatial association between subsurface resistivity anomalies and groundwater chemistry. Geoelectrical models showed laterally extensive conductive zones (10–50 Ωm) from near-surface depths to ~15.9 m, consistent with a preferential migration of the effluent through the permeable coastal plain sands. Hydrochemical analyses indicated deterioration of groundwater quality near the processing area with acidic conditions (pH 4.9), high total dissolved solids (1085 mg/L), cyanide concentrations up to 2.95 mg/L, high biochemical and chemical oxygen demands (142 and 285 mg/L, respectively) and elevated iron and manganese concentrations, while independent VES models identified conductive horizons which provided complementary vertical control. Water quality gradually improved with increasing distance from the processing area, with the WQI decreasing from 96.8 (Very Poor) at 15 m to 47.1 (Good) at 350 m. Piper analysis revealed a mixed Ca-Mg-Na-Cl-HCO 3 hydrochemical facies. The correlation of geophysical and hydrochemical observations supports an integrated approach for characterising conductive subsurface zones and related groundwater-quality conditions.

Keywords: Electrical Resistivity Tomography; Vertical Electrical Sounding; Groundwater Contamination; Cassava Effluent; Hydrochemistry; Water Quality Index.

1.0 Introduction

Groundwater is the primary source of water for domestic, agricultural and industrial purposes in Nigeria, particularly in the rural areas where surface water is scarce or seasonally unavailable (Salami & Ogbamikhumi, 2017; Itsueli et al., 2026). Groundwater accounts for approximately 30 % of the world's fresh water and is often viewed as being more protected from surface pollutants than surface water resources (Foster et al., 1998; Morris et al., 2003). However, in Nigeria, approximately 39% of the rural population has access to potable water and the quality of available groundwater is progressively degrading due to anthropogenic activities (Federal Republic of Nigeria, 2002; UNICEF/WHO, 2019). Agricultural and industrial activities, in which effluents are discharged, may lead to the infiltration of contaminants into the groundwater system with serious risks to human health and ecosystem integrity (Awomeso et al., 2010; Forster et al., 1998; Rahman & Singh, 2019). Cassava (Manihot esculenta Crantz) is one of the most important staple food crops in sub-Saharan Africa, with Nigeria being the largest producer in the world, surpassing Brazil by a third and nearly doubling the production of Indonesia and Thailand (Chibuzor, 2024), contributing to more than 20% of the total world production (FAO, 2020).

Cassava processing to garri, fufu, starch and flour generates large volumes of effluent containing high levels of biochemical oxygen demand (BOD), chemical oxygen demand (COD), organic matter, cyanogenic glycosides (linamarin and lotaustralin) and suspended solids (Emagbetere et al., 2018; Olayinka, 2013). Cassava processing mills are known to be one of the major sources of ground water pollution in the Niger Delta region (Adigun & Olorunfemi, 2017; Okunade & Adakalu, 2013). Wastewater is largely disposed of untreated in open fields, gutters or surface water bodies where it percolates through the soil profile and pollutes shallow aquifers (Omotioma et al., 2013).

The environmental chemistry of cassava effluents is particularly alarming. During processing, the endogenous linamarase hydrolyses the cyanogenic glycosides to release hydrogen cyanide (HCN) that dissociates in water to form cyanide ions (CN-) and other cyanogenic compounds (Ekpechi, 1994; Okafor et al., 2015). The effluents are also rich in organic acids (acetic, formic, propionic), reducing sugars, proteins and minerals that increase the ionic strength and electrical conductivity of infiltrating water (Emagbetere et al., 2018). The chemical composition of these effluents provides them with a high conductivity and thus makes it possible to detect them by electrical geophysical methods.

Electrical resistivity tomography (ERT) is a non-invasive geophysical method that produces high resolution images of the resistivity distribution in the subsurface (Ighodalo & Airen 2024; Ighodalo & Ohioma 2024), and thus, is very useful in mapping of contaminant plumes where there are contrasts in the conductivity between the polluted and pristine zones (Amidu & Olayinka, 2006; Loke et al., 2013). The method has been successfully used to delineate leachate plumes from landfills (Ighodalo & Okanigbuan, 2022; Iyoha et al., 2020), industrial contamination (Aizebeokhai & Oyeyemi, 2014) and agro-industrial pollution (Ehilenboadiaye et al., 2018; Ighodalo & Japhet, 2024). The merging of 2-D profiles to 3-D volumes enables complete visualisation of the plume geometry, thickness variation and lateral continuity (Alile et al., 2017a, 2017b).

But geophysical imaging alone cannot determine the specific contaminants and cannot quantify their concentration. The coupling of geophysical data with the geochemical analysis of water and soil samples constitutes a key validation which allows: (1) to identify the specific contaminants and their sources, (2) to quantify the level of pollution in accordance with the standards of regulations, (3) to correlate the geophysical anomalies with the measured chemical parameters, and (4) to assess the environmental risks in a robust way (Cosenza et al., 2006; Samouelian et al., 2005). The value of the combination of geophysical methods with hydrochemical and soil geochemical analysis for a comprehensive assessment of contamination has been demonstrated by Adigun and Olorunfemi (2017), Emagbetere et al. (2018) and Rahman and Singh (2019).
Although the need for integrated approaches is acknowledged, studies that have integrated ERT with systematic geochemical analyses of groundwater and soil for assessing contamination from cassava effluent are scarce in the Niger Delta. This study fills this gap by combining 2-D/Quasi-3-D resistivity visualisation and physicochemical analysis of hand-dug well water to: (1) determine the spatial extent and 3-D geometry of contaminant plumes; (2) quantify the degree of groundwater contamination; (3) develop quantitative relationships between geophysical signatures and geochemical parameters; and (4) assess environmental risk and suggest mitigation measures.

2.0 Location and Geology of the Study Area

Ugbolu is located about 10 km northeast of Asaba, the capital city of Delta State Nigeria. It lies between latitude 6° 17′ N and 6° 21′ N and longitude 6° 43′ E and 6° 47′ E (Figure 1). The dominant geology of Ugbolu is Benin Formation (Coastal Plain Sands) which is part of the large Niger Delta sedimentary basin (Short & Stauble, 1967). The Benin Formation consists of unconsolidated to poorly

consolidated, friable sands, sandy clays and occasional gravel lenses with high primary porosity (25–40%) and permeability (hydraulic conductivity 10^{-4} to 10^{-3} m/s) (Reyment, 1965; Oteri & Atolagbe, 2003). It is normally 100–1,500 m thick and represents the most prolific aquifer system in the Niger Delta.e Niger Delta sedimentary basin (Short & Stauble, 1967). The Benin Formation is characterized by unconsolidated to poorly consolidated, friable sands, sandy clays, and occasional gravel lenses, with high primary porosity (25–40%) and permeability (hydraulic conductivity 10^{-4} to 10^{-3} m/s) (Reyment, 1965; Oteri & Atolagbe, 2003). The formation is typically 100–1,500 m thick and constitutes the most prolific aquifer system in the Niger Delta.

The surficial geology comprises lateritic sandy loam (0–2 m depth), underlain by yellowish-brown to grey, medium to coarse-grained sand (2–15 m), with discontinuous clay lenses (0.5–3.0 m thick) at variable depths. The high permeability of these sands facilitates rapid vertical and lateral migration of infiltrating contaminants, making the shallow aquifer highly vulnerable to surface pollution (Adigun & Olorunfemi, 2017). The water table occurs at depths of 2.5–8.5 m, with seasonal fluctuations of 1.5–3.0 m. Groundwater in the study area is exploited through shallow hand-dug wells (depth 5–15 m) and medium-depth boreholes (depth 20–45 m). The hand-dug wells are particularly vulnerable to contamination due to their shallow depth, lack of sanitary seals, and proximity to pollution sources.

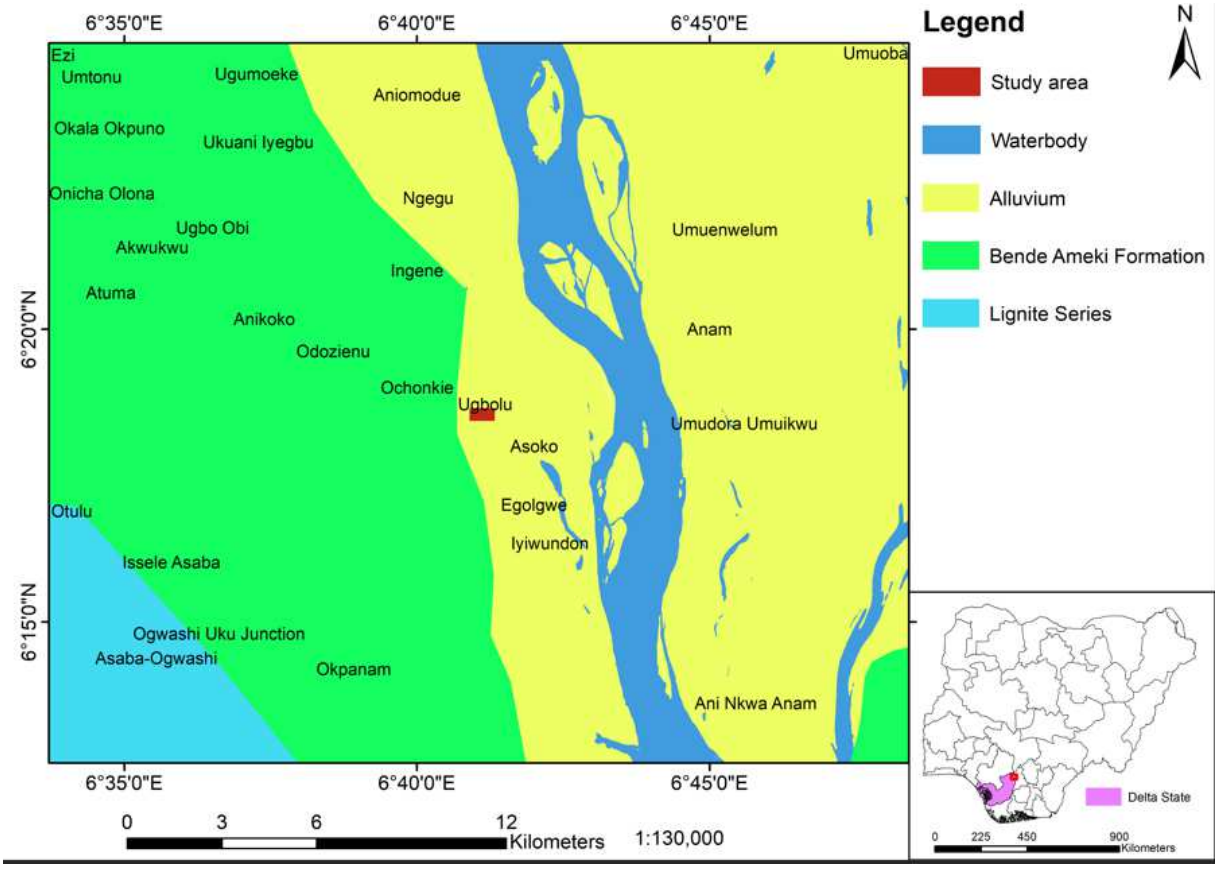


Figure 1: Map showing location and Geology of the study area

The climate is tropical monsoon (Köppen Am), with mean annual rainfall of 1,800–2,200 mm concentrated in a wet season from April to October. Mean annual temperature is 27.5°C, with relative humidity averaging 85%. The high rainfall intensity facilitates rapid infiltration of surface contaminants into the shallow aquifer. The area is drained by seasonal streams and tributaries of the Niger River system.

3.0 Materials and Methods

Geophysical Investigation

Ten ERT traverses, each of length 100 m were established across the study area to cover the zones of active cassava processing and effluent discharge. The traverses were orientated both perpendicular and parallel to the dominant groundwater flow direction (ca. NNW-SSE) at 20–50 m spacing depending on the accessibility of the site and the distribution of the mills. The Wenner–Schlumberger array was chosen because it has the best sensitivity to both vertical and horizontal changes in resistivity, which is important for imaging conductive leachate plumes in heterogeneous subsurface conditions (Dahlin & Loke, 1998; Aizebeokhai et al., 2010).

Data acquisition employed a PASI Earth Resistivity Meter with 21 stainless steel electrodes per traverse at 5 m spacing. Saline water solution was applied around electrode bases in dry areas to ensure good electrical contact and reduce contact resistance to < 2 kΩ. A known current (I) was injected through current electrodes, and the resulting potential difference (V) was measured between potential electrodes. Apparent resistivity (ρa) was calculated as:

$$\rho a = K \times V/I \quad (1)$$

where K is the geometric factor for the Wenner–Schlumberger array:

$$K = \pi n(n+1)a \quad (2)$$

where a is the minimum electrode spacing (5 m) and n is the integer separation factor.

Measurements were taken for increasing values of n (1–6) to achieve deeper subsurface penetration, yielding a quasi-2-D resistivity dataset with 6 depth levels. The maximum investigation depth was approximately 15.9 m.

Data processing and inversion were performed using RES2DINV software (Loke, 2010), employing a smoothness-constrained least-squares inversion algorithm. The objective function minimized during inversion was:

$$\Phi(m) = ||W_d(d_{obs} - d_{cal})||^2 + \lambda^2 ||W_m(m - m_{ref})||^2 \quad (3)$$

where d_{obs} is observed data, d_{cal} is calculated data, m is model parameters, W_d is data weighting matrix, W_m is model roughness matrix, λ is damping factor, and m_{ref} is reference model. Inversion quality was assessed using root-mean-square (RMS) error, with acceptance criteria of RMS < 10% for environmental investigations.

Quasi-3-D resistivity visualization Visualization

Quasi-3D resistivity visualisation

Interpolation of 2-D inverted resistivity sections between parallel traverses was performed with Voxler 4 using a kriging technique to produce a quasi-3-D resistivity volume. Depth slices at 1 m intervals and isosurfaces at 10, 25, 50 and 100 Ωm were created to visualise the spatial distribution of conductive zones.

Vertical Electrical Sounding (VES)

Ten Vertical Electrical Sounding (VES) stations were established across the study area using the Schlumberger electrode configuration to complement the vertical control of the resistivity structure from the ERT. A transect with the VES stations was established from the cassava mill (VES-01 at 5 m) to 480 m from the mill (VES-10) providing spatial coverage overlapping the ERT traverses. Schlumberger array was chosen for better depth resolution and thin layer resolution which is essential to identify the shallow contaminated zone. The electrode spacing (AB) was in the range of 2 m to 200 m, and the potential electrode spacing (MN) increased from 0.5 m to 20 m with increasing AB.

The apparent resistivity was estimated by using the standard Schlumberger geometric factor. VES data were interpreted through the curve matching with master curves and computer assisted iterative inversion (IpI2win software) to obtain layered earth models. Each station was interpreted as a multi-layer geoelectric section of topsoil, contaminated zone, weathered sand, fresh sand aquifer and basal clayey sand. Curve type, layer thickness and resistivity were compared to ERT depth sections for validation of the geophysical interpretation.

Hydrochemical Sampling and Analysis

Five hand-dug wells (HW-01 to HW-05) were selected for groundwater sampling based on their spatial distribution relative to the cassava processing mill and their location within or near the ERT-identified low-resistivity zones. The wells range in depth from 8.5 m to 14.0 m and are situated at distances of 15 m, 45 m, 120 m, 200 m, and 350 m from the effluent discharge point.

Water samples were collected in pre-cleaned polyethylene bottles according to standard sampling protocols (APHA, 2017). pH, Electrical Conductivity (EC) and temperature were measured in-situ, using a calibrated portable multi-parameter probe. Turbidity was determined by nephelometric turbidimeter.

Laboratory analyses were conducted for the following parameters: major cations (Ca^{2+}, Mg^{2+}, Na^{+}, K^{+} by flame photometry and EDTA titration); major anions (HCO_3^{-}, CO_3^{2-}, Cl^{-}, SO_4^{2-}, NO_3^{-} by titration and spectrophotometry); organic parameters (Chemical Oxygen Demand, Biochemical Oxygen Demand, Total Organic Carbon); trace metals (Fe, Mn, Zn by Atomic Absorption Spectrophotometry); cyanide by colorimetric method using pyridine-barbituric acid reagent; Total Dissolved Solids calculated from EC; and Total Hardness and Alkalinity by titrimetric methods.

All analyses were performed at the Department of Physics and toxicology Laboratories, University of Benin. Quality assurance included blank samples, duplicate analyses, and calibration with certified reference standards.

Water Quality Index (WQI) Computation

The Water Quality Index was calculated for each well using the weighted arithmetic index method of Brown et al. (1972), which integrates several physico-chemical parameters into a single numerical value representing overall water quality. Fourteen parameters were chosen according to their importance in

contamination of cassava effluent and effects on human health: pH, TDS, turbidity, COD, BOD_5, cyanide, nitrate, sulphate, chloride, iron, manganese, zinc, total hardness and alkalinity.

The WQI is calculated as:

$$WQI = \Sigma(q_i \times w_i) / \Sigma w_i \quad (4)$$

where q_i is the quality rating for the i-th parameter and w_i is the unit weight.

For most parameters (undesirable), the quality rating is:

$$q_i = [(V_n - V_i) / (V_n - V_0)] \times 100 \quad (5)$$

For pH (desirable with a range):

If $V_i \leq 7.0$: $q_i = [(V_i - 6.5) / (7.0 - 6.5)] \times 100$

If $V_i > 7.0$: $q_i = [(8.5 - V_i) / (8.5 - 7.0)] \times 100$

where V_i = Observed value, V_0 = Ideal value, and V_n = Permissible value (WHO/NSDWQ standard).

The unit weight w_i for each parameter was assigned based on relative importance, with higher weights given to health-critical parameters (cyanide, TDS) and lower weights to less critical parameters (zinc, alkalinity). The WQI classification follows the standard scheme: Excellent (0–25), Good (26–50), Poor (51–75), Very Poor (76–100), and Unsuitable (>100).

Geochemical Facies Analysis

Major ion data were converted to milliequivalents per litre (meq/L) and plotted on a Piper trilinear diagram to determine the hydrochemical facies of the groundwater. The Piper diagram enables the classification of water types based on the relative proportions of cations (Ca^{2+}, Mg^{2+}, $Na^+ + K^+$) and anions (HCO_3^-, Cl^-, $SO_4^{2-} + NO_3^-$). Charge balance errors were computed to verify analytical accuracy, with acceptable limits set at ±5%.

4.0 Results

Two-Dimensional ERT Results

The inverted resistivity sections have values varying between 4.12 to 11,948 Ωm. The RMS errors are 3.1-12.3%. The profiles are extended to a depth of ~15.9 m with an electrode spacing of 5 m, exhibiting variable inversion-fit quality between the profiles.
Several low resistivity anomalies (10 – 50 Ωm) were delineated across the study area, and interpreted as conductive plumes of cassava effluent leachate. These plumes are seen at shallow depths (1.6-12.5 m), with some extending to the maximum depth investigated (15.9 m). The shapes of the plumes are continuous and discontinuous. They occur mainly in the permeable sandy units of the Benin Formation. The zones of high resistivity (> 100 Ωm) indicate relatively competent lateritic and weathered layers at deeper levels, which hampered the vertical migration to a certain degree. The spatial continuity of the conductive anomalies over several traverses confirms the lateral spread of contamination over the study area.
The individual 2-D profiles show the following:

Profile 1: This line located immediately down-gradient of the largest processing mill showed one large low-resistivity anomaly (10–45 m) that extended laterally from 0–45 m and to the maximum depth of investigation of 15.9 m (Figure 2 A). It is interpreted as a mature, vertically extensive leachate plume due to long-term effluent discharge. Relatively uncontaminated conditions are indicated by high-resistivity zones (> 500 Ωm) at 55–100 m lateral distance.

Profile 2: Central part (30-75 m) was dominated by a wide low-resistivity zone (4.12-40.2 Ωm) that

extended to a depth of 15 m. Localised high-resistivity features (1,225–11,948 Ωm) at 15–25 m and 70–75 m (Figure 2B) indicate lateritic or compacted sandy units with low contamination. The RMS error of 5.1% indicates an excellent quality of inversion.

Profile 3: Localised shallow low-resistivity anomaly (7.32–37.6 Ωm) at 2–7 m depth and 20–40 m laterally, interpreted as a localised plume from a point discharge (Figure 2C). The underlying high-resistivity zone (> 437 Ωm) implies limited vertical migration which may be caused by a clay lens or compacted layer.

Profile 4: Showed a shallow conductive zone (18.9–354 Ωm) from 0–35 m in lateral extent, with a depth of 8 m and a sharp boundary to moderate-resistivity materials (153–354 Ωm) at 60–100 m. (Fig. 2D). This gradation suggests lateral plume migration from west to east.

Profile 5: The western part (0–60 m) was characterised by low resistivity (<51 Ωm) down to 6–8 m depth, which we interpreted as widespread surface contamination. High resistivity anomaly (> 189 Ωm) at 70-95 m (Fig. 2E). represents a relatively clean sandy or lateritic zone.

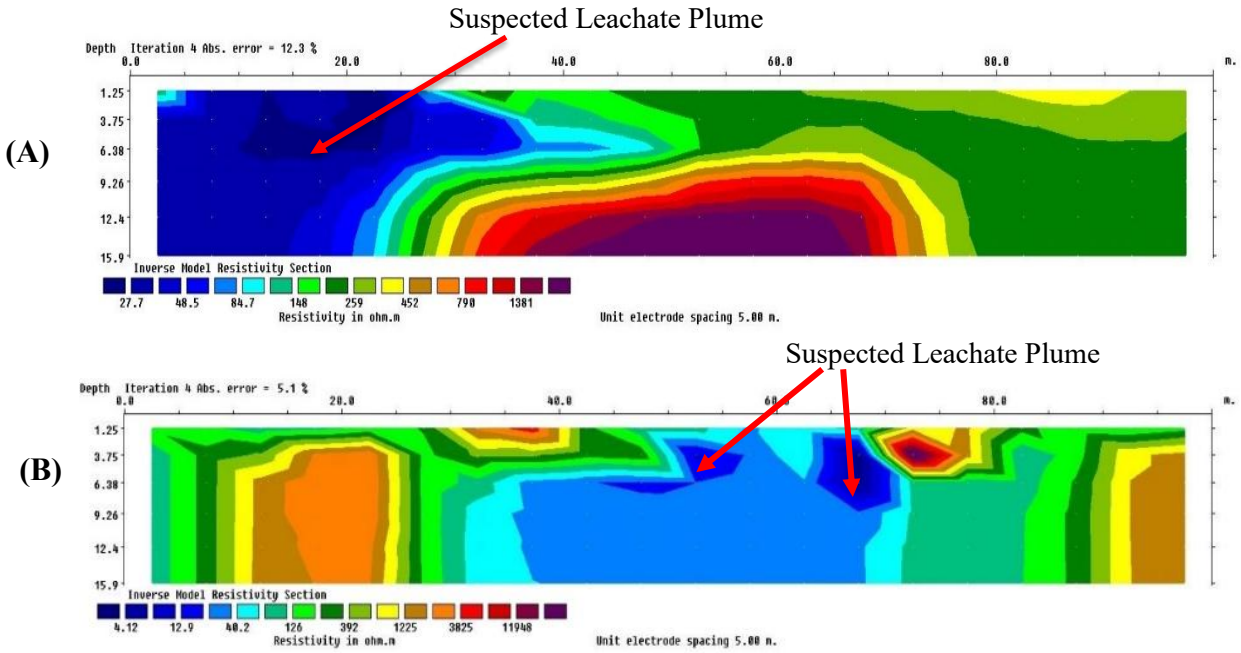
Profile 6: Two discrete conductive zones at 20–45 m and 65–85 m (< 47.2 Ωm) (Figure 2F) indicate multiple discharge points or bifurcated plume migration along permeable pathways.

Profile 7: This profile had a large conductive anomaly (9.06–62.5 Ωm) from surface to 10 m depth at 60–75 m depth, with high-resistivity materials (> 431 Ωm) on the eastern side (Figure 2G). The strong resistivity anomaly suggests localised contamination from a point source.

Profile 8. The majority part of the profile showed low resistivity (< 75.5 Ωm) indicating a wide spread of areal contamination. The thin high-resistivity layer at 70–80 m may represent compacted less weathered material that temporarily impedes contaminant migration near the surface.

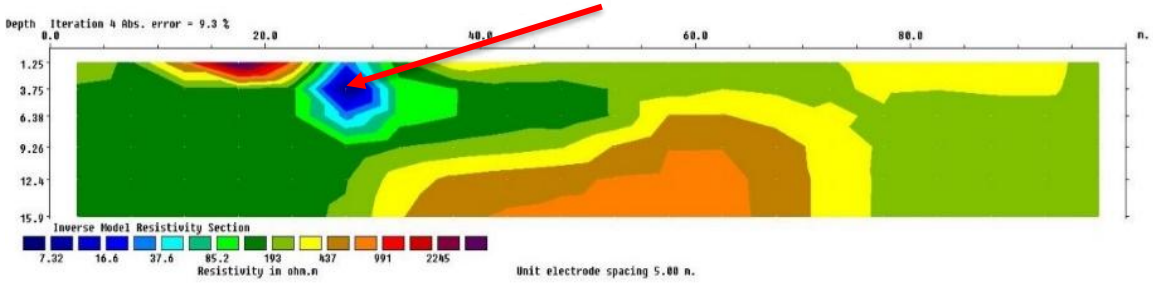
Profile 9: The western half showed a large conductive zone to maximum depth (< 50 Ωm) interpreted as highly contaminated due to long-term infiltration. The eastern half exhibited moderate to high resistivity (> 261 Ωm) with a sharp contact indicating limited lateral migration.

Profile 10: Showed a unique pattern with a central high-resistivity anomaly (35-75 m) encircled by low-resistivity zones (< 52.4 Ωm) at both extremities. A key feature is believed to be a geological barrier (possibly a clay ridge or cemented laterite) that has prevented contaminant migration.



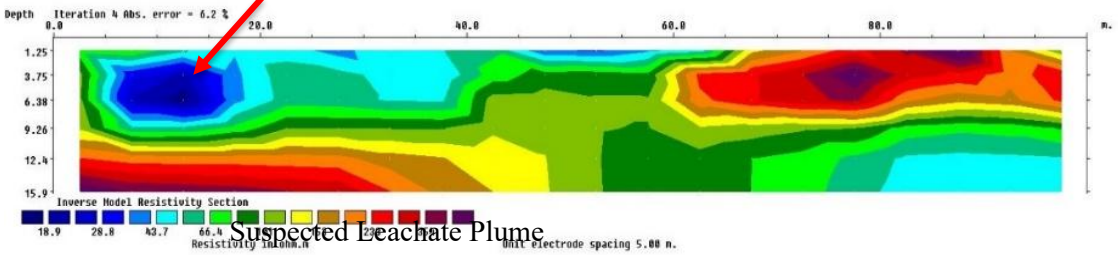
Suspected Leachate Plume

(C)



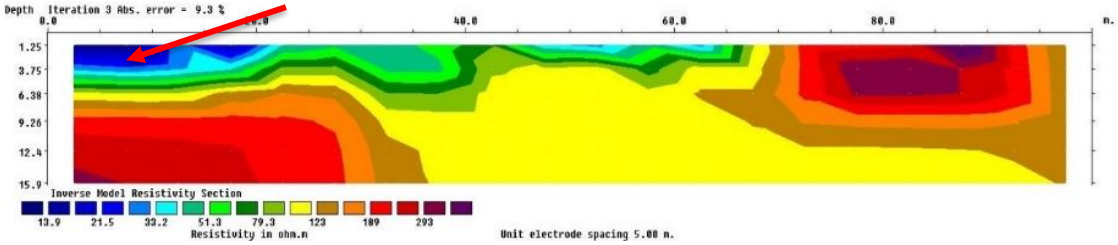
Suspected Leachate Plume

(D)



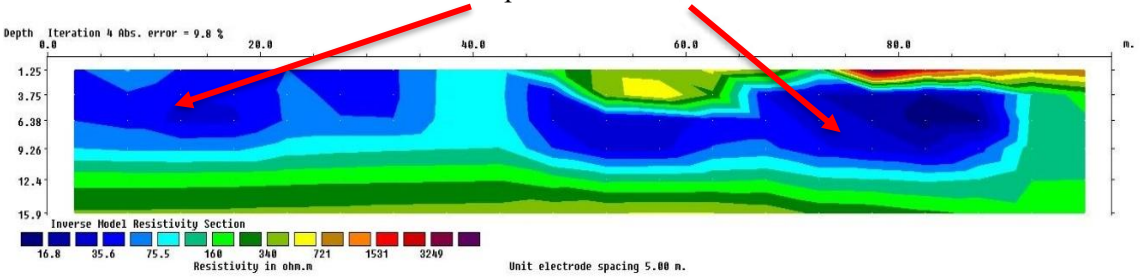
Suspected Leachate Plume

(E)



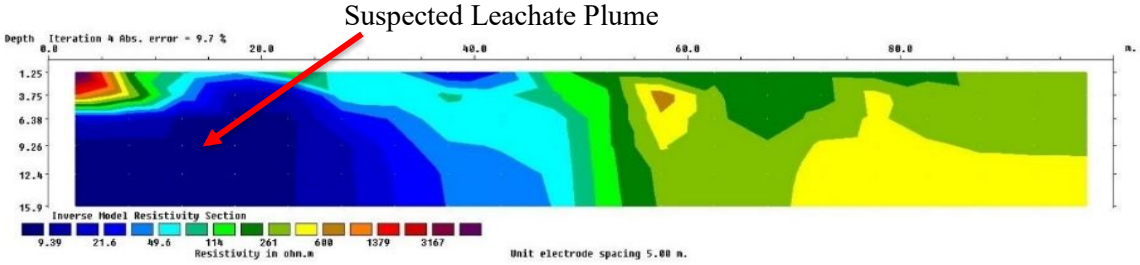
Suspected Leachate Plume

(F)



Suspected Leachate Plume

(G)



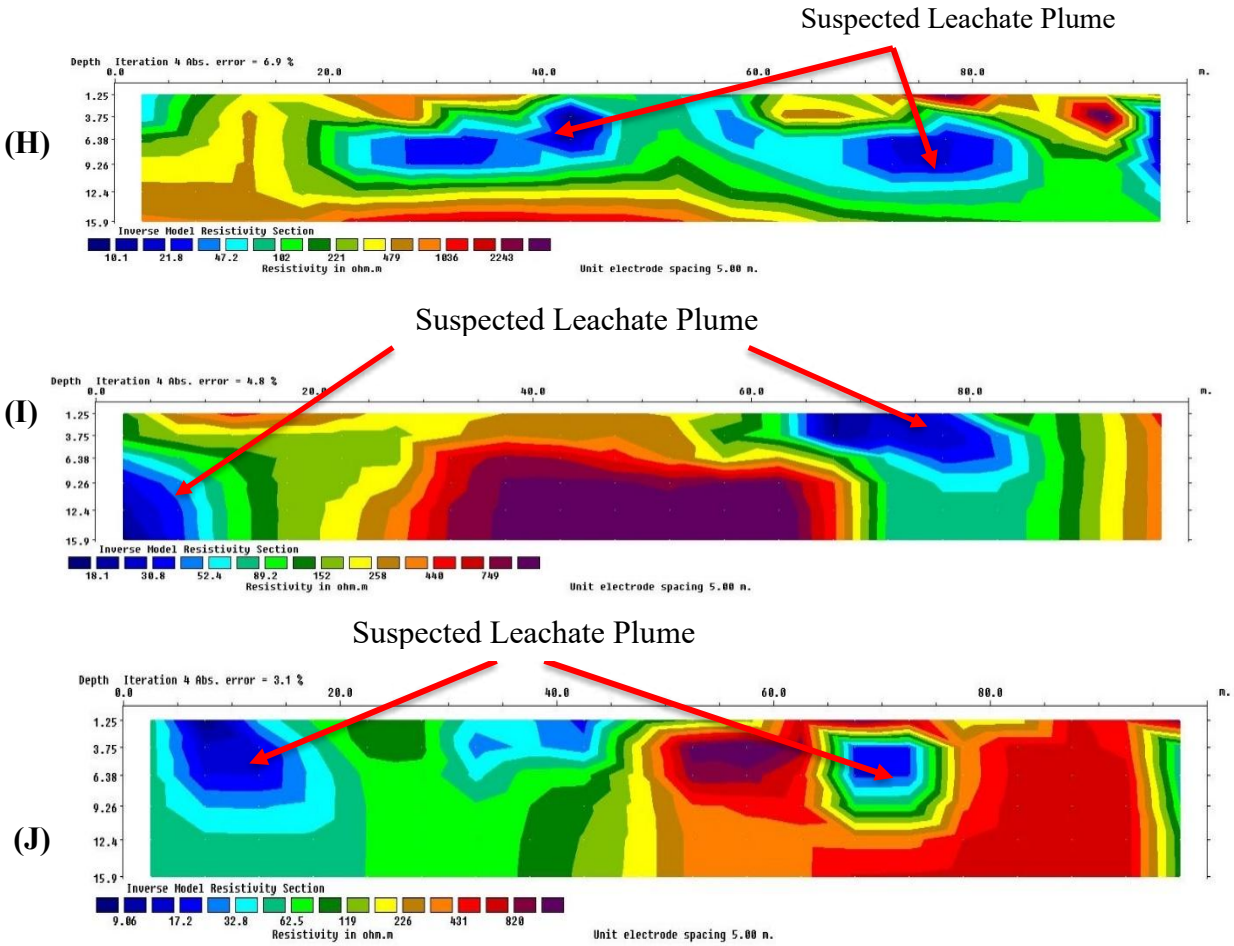


Figure 2 (A to J): Inverted Model of 2-D ERT along Profile (1-10)

Quasi-3-D resistivity Visualization

The Quasi 3-D resistivity model provides a complete volumetric picture of the contaminant distribution under the cassava processing site (Figure 3a). Resistivity values range from a few 20 Ωm to over 6,000 Ωm. The model reveals several low-resistivity zones (blue colours) distributed across the site, representing areas where cassava effluent has infiltrated and accumulated within the subsurface. The irregular geometry of the anomalies suggests that contaminant migration is controlled by variations in soil permeability, moisture content, and subsurface stratigraphy. The iso-surface model highlights the spatial extent of contamination, showing multiple interconnected conductive bodies extending both laterally and vertically. These zones correspond to preferential pathways through which effluent migrates into the subsurface. Depth slices indicate that contamination is most intense within the shallow subsurface (0–10 m) (Figure 3b - e), where effluent discharge occurs. Resistivity generally increases away from the source areas, suggesting dilution and attenuation of contaminants with distance .

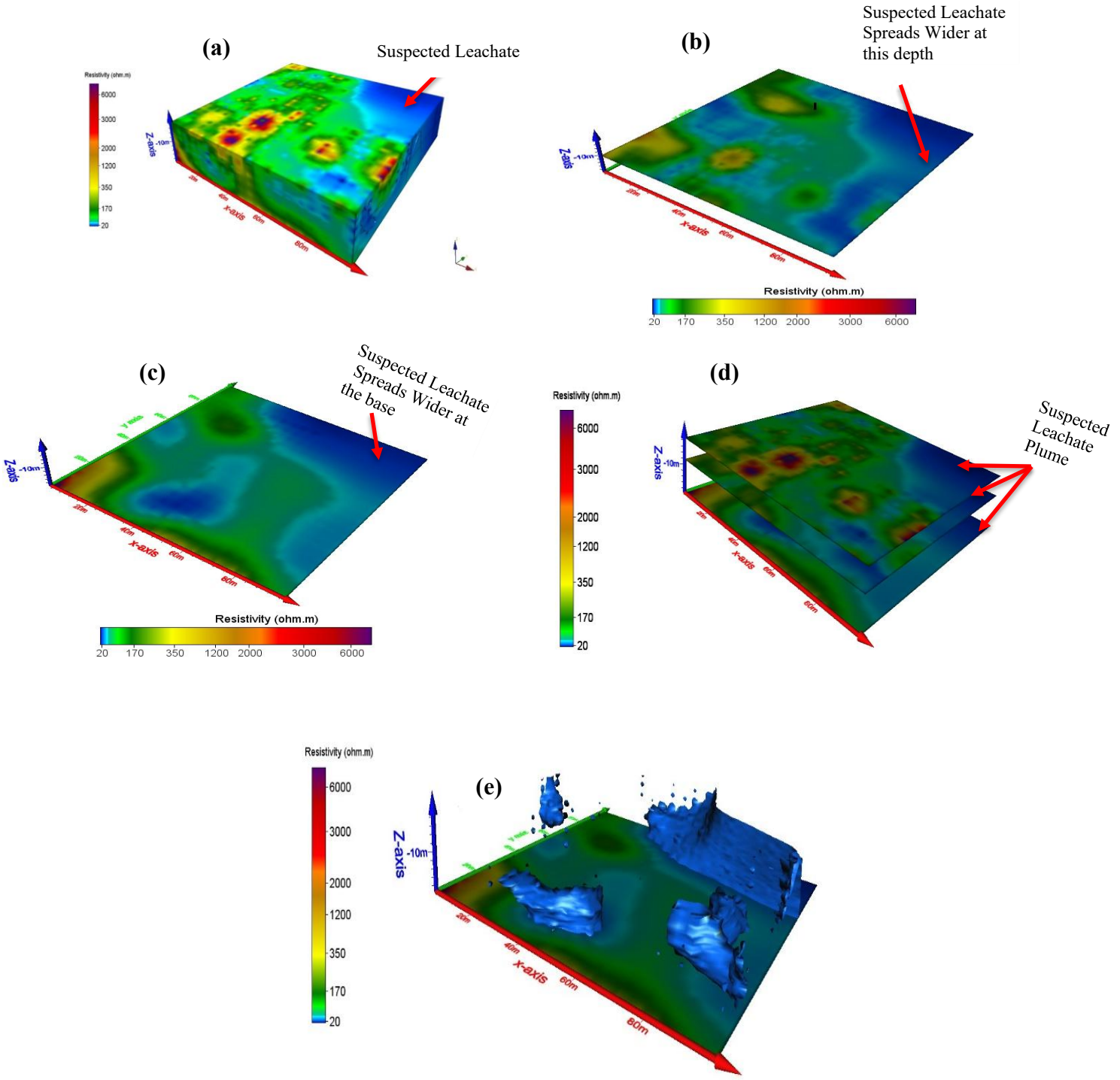


Figure 3 (a-e): Quasi-3-D resistivity visualization showing (a) block volume, (b) depth slice at 10m and (c) depth slice at 15.9 m (d) multiple depth slice at 15.9 m (e) isosurface distribution of conductive zones.

Vertical Electrical Sounding (VES) Results

The ten VES stations exhibit mixed curve types (HKA, AHA, HA, HK, HA, HAH, KA, AHA, HA, KA), reflecting variable subsurface resistivity structures within the Benin Formation. The interpreted five-layer geoelectric models are presented in Table 1.

Table 1: VES Layer Parameters

VES Station	L1 Depth (m)	L1 ρ (Ω m)	L2 Depth (m)	L2 ρ (Ω m)	L3 Depth (m)	L3 ρ (Ω m)	L4 Depth (m)	L4 ρ (Ω m)	L5 Depth (m)	L5 ρ (Ωm)	Curve Type
VES-01	0.00–0.50	35.8	0.50–1.02	20.05	1.02–3.06	12.5	3.06–8.96	47.9	>8.96	691	**HKA**
VES-02	0.00–0.50	14.18	0.50–1.15	25.14	1.15–6.95	41.8	6.95–18.15	51.05	>18.15	642	**AHA**
VES-03	0.00–0.50	71.4	0.50–1.08	21.9	1.08–5.98	36.9	5.98–16.78	111	>16.78	328	**HA**
VES-04	0.00–0.50	44.4	0.50–1.12	49.3	1.12–6.62	55.5	6.62–18.72	1006	>18.72	668	**HK**
VES-05	0.00–0.50	88.2	0.50–1.05	50.9	1.05–5.75	714	5.75–17.05	60.2	>17.05	791	**HA**
VES-06	0.00–0.50	118	0.50–1.10	**115**	1.10–6.20	206	6.20–17.70	1626	>17.70	127	**HAH**
VES-07	0.00–0.50	62.2	0.50–1.13	373	1.13–6.73	132	6.73–17.23	113	>17.23	360	**KA**
VES-08	0.00–0.50	413	0.50–1.09	441	1.09–5.89	599	5.89–16.79	90.2	>16.79	350	**AHA**
VES-09	0.00–0.50	121	0.50–1.14	78.4	1.14–6.44	147	6.44–18.24	191	>18.24	502	**HA**
VES-10	0.00–0.50	47.1	0.50–1.06	64.1	1.06–5.66	21.5	5.66–15.86	182	>15.86	345	**KA**

Layer 1 (Depth 0.00–0.50 m)

The first layer has resistivity values ranging from 14.18 Ωm to 413 Ωm (mean = 101.5 Ωm) and is interpreted as the topsoil layer, which is mainly composed of lateritic sand, sandy clay and organic-rich surface materials. Changes in resistivity indicate changes in moisture content, clay content and surface conditions. The low resistivity value at VES-02 (14.18Ωm) might be a consequence of the effluent infiltration into the near surface soil horizon.

Layer 2 (Depth 0.50-1.02 to 1.15 m)

The second layer is characterised by resistivity values between 20.05 Ωm and 441 Ωm (mean = 123.9 Ωm) and is interpreted as moist sandy clay to clayey sand. Four stations (VES-01, VES-02, VES-03, VES-10) have resistivities less than 50 Ωm which could indicate increased conductivity due to increased moisture content and possible contaminant infiltration. This layer provides the first conduit for cassava-effluent leachate to migrate downwards into the subsoil. The thickness of this layer varies from 1.02 m at VES-01 to 1.15 m at VES-02, indicating local variations in the thickness of the topsoil.

Layer 3 (1.02–3.06 to 1.15–6.95 m Depth)
The third layer has a high resistivity range (12.5 Ωm to 714 Ωm, mean = 196.6 Ωm) which indicates a high lateral lithological variation. Four stations (VES-01, VES-02, VES-03, VES-10) have resistivity values less than 50 Ωm and are interpreted as contaminated weathered sand or sandy clay saturated with conductive leachate. Conversely, the high resistivity zones of VES-05 (714 Ωm) and VES-08 (599 Ωm) indicate relatively clean and competent sandy formations. This layer corresponds to the main contaminated horizon in the study area. The base of this layer ranges from 3.06 m (VES-01) to 6.95 m (VES-02) and the majority of the stations are between 5.66 and 6.73 m.

Layer 4 (Depth 3.06–8.96 to 6.62-18.72 m)
The fourth layer has resistivity values from 47.9 Ωm to 1626 Ωm (mean = 347.8 Ωm) and is interpreted as a weathered to partially consolidated sand unit. Four stations (VES-01, VES-02, VES-05, VES-08) have resistivity values below 100 Ωm indicating the contaminant migration to deeper subsurface. However, the high resistivity values of VES-04 (1006 Ωm) and VES-06 (1626 Ωm) suggests relatively uncontaminated sandy deposits with low ionic concentrations. This layer is a transitional zone between the contaminated shallow subsurface and the deeper aquifer. The thickness of this layer varies from 8.96 m at VES-01 to 18.72 m at VES-04 which is consistent with the variation thickness of the overlying units.

Layer 5 (>8.96 to >18.72 m Depth)
The fifth layer has resistivity values from 127 to 791 Ωm (mean = 480.4 Ωm) and is interpreted as the main freshwater-bearing coarse sand aquifer of the Benin Formation. High resistivity values indicate generally good conditions of ground water and low concentrations of dissolved contaminants. The shallowest aquifer is at VES-01 (>8.96 m) and is also the most vulnerable to surface contamination. The deepest aquifer top is at VES-04 (>18.72 m) and thus it has the highest protection. The lowest resistivity of VES-06 (127 Ωm) could indicate areas where the contamination has begun to move downwards or areas with clay intercalations within the aquifer. The aquifer depth varies across the study area by 9.76 m indicating variable thickness of the overlying contaminated units.

hydro chemical Results
Table 2: physico-chemical parameters of hand-dug wells at varying distances from the cassava processing mill.

Parameter	HW-01 (15 m)	HW-02 (45 m)	HW-03 (120 m)	HW-04 (200 m)	HW-05 (350 m) control	Mean ± SD	CV (%)	WHO Limit	NSDWQ Limit
Depth (m)	12.5	10.2	14.0	8.5	11.3	11.3 ± 2.1	18.7	-	-
pH	**4.9**	**5.2**	**5.6**	**6.5**	**6.7**	5.52 ± 0.50	9.0	6.5–8.5	6.5–8.5
EC (µS/cm)	**1350**	**1220**	890	720	580	952 ± 326	34.3	1500	1500
TDS (mg/L)	**1085**	**910**	**570**	333	243	628 ± 363	57.8	500	500
Turbidity (NTU)	**45.2**	**32.8**	**18.5**	**8.2**	4.5	21.8 ± 17.1	78.1	5	5
BOD_5 (mg/L)	**142**	**98**	**106**	**87**	**74**	101.4 ± 25.7	25.3	Not specified	Not specified
COD (mg/L)	**285**	**261**	**208**	**170**	**170**	218.8 ± 52.5	24.0	Not specified	Not specified
Cyanide (mg/L)	**2.95**	1.05	**0.09**	ND	ND	1.45 ± 1.96	135.4	0.05	0.05

BOD_5/COD	0.498	0.375	0.510	0.512	0.435	0.466 ± 0.055	11.8	-	-

Hydrochemical data from the five sampled wells display a consistent directional trend with distance from the mill, corroborating the plume geometry delineated by ERT and VES. While the limited number of sampling points (n = 5) precludes robust statistical inference, the observed trends align with the geophysical anomalies and are consistent with established attenuation processes for organic-rich leachates in permeable coastal plain sands. which is indicative of a plumes of contamination with a point source discharge moving through a shallow unconfined aquifer.

pH and Acidification. The pH of the most proximal well (HW-01, 15 m) is 4.9 and three of five wells are below the minimum limit of 6.5 set by WHO/NSDWQ. The pH exhibits a near-linear recovery trend with distance from the source, increasing from 4.9 to 6.7 across the transect, indicating progressive neutralization of organic acids (acetic, formic, hydrocyanic) by the carbonate-poor but silicate-buffered matrix of the Benin Formation. The acid front is geochemically important since it initiates secondary contamination processes such as reductive dissolution of Fe- and Mn-oxyhydroxides (Table 3) and carbonate speciation (Table 5).

Electrical Conductivity (EC), **and Total Dissolved Solids (TDS)**. EC and TDS both decrease markedly with distance from the mill, consistent with progressive dilution of the conductive effluent plume, with the attenuation of EC being the primary control on attenuation of bulk conductivity. Within 45 m of the mill both parameters are over NSDWQ standards. One feature of particular interest is that the TDS/EC ratio decreases as a function of distance from the source, from 0.80 at 15 m to 0.42 at 350 m, reflecting an altered signature from an organic-rich near-source signature to a more mineralized, geogenically driven signature downgradient where biodegradable organics have been attenuated.

Turbidity. The decrease in turbidity from 45.2 NTU (HW-01) to 4.5 NTU (HW-05) represents a 90% reduction with a half-distance of ~99 m, indicating two possible mechanisms: (i) physical removal of PM from the effluent due to filtration in the sandy vadose zone; and (ii) destabilization of particles due to colloids in the effluent and settling when it mixes with groundwater. HW-01 is very turbid, reflecting either direct or relatively little pre-treatment of raw effluent by soil.

Organic Loading (BOD_5 and COD)

The spatial pattern for both BOD_5 and COD shows a heavy organic loading near the mill, however the pattern is not a monotonous decay. This rules out any one phase, first-order attenuation model for the transect in general.

COD decreases from 285 mg/L (HW-01) to 170 mg/L (HW-04), but then plateaus at 170 mg/L through HW-05 (350 m). The lack of change over the last 150 m suggests a change in labile organics from rapid initial removal (0-200m) to a recalcitrant fraction that will not be removed over the sampled transect. Since the limit values for COD are not specified in the table, a claim to standard exceedance cannot be confirmed based on these data alone.

BOD_5 follows an even more irregular path: 142 → 98 → 106 → 87 → 74 mg/L. The distance decay between 45 m (HW-02) and 120 m (HW-03) is not maintained and is considered a break. As such, the BOD_5 data cannot be reliably fitted with a first order decay constant, or one half-distance. There is evidence of localized heterogeneity, as indicated by the elevated concentration at HW-03, where either

the concentration of organic matter is high, or where the groundwater is mixed differently, or where the microbial activity is higher than at other sites and causes a transient increase in biodegradable oxygen demand despite the greater lateral distance from the source. This complexity is also supported by the BOD_5/COD ratio. The ratio decreases to a minimum at HW-02 (0.375) as expected for preferential mineralization of labile organic fraction in the top 45 m. However, it then rebounds sharply to 0.510 at HW-03 and 0.512 at HW-04 before falling again to 0.435 at HW-05. The non-monotonic behavior is not predicted by the depth of the wells alone, as the ratios of HW-03 (14.0 m, deepest), HW-04 (8.5 m, shallowest) are essentially the same, while the ratio of HW-05 (11.3 m, intermediate depth) is lower. In this data set, depth is therefore not a useful indicator of the organic character.
Synthesis: The data suggest a carbohydrate rich effluent which begins to quickly degrade, but with aquifer heterogeneity and the production of a persistent organic residue distorting the attenuation trajectory. The plateau in the COD data (from 200 m to 350 m) shows that a persistent organic footprint occurs at least up to the control well and possibly further. The most parsimonious explanation is a mixture of labile and recalcitrant organics at 200 m depth and a residual of poorly biodegradable organics at 350 m depth; however, the rate of attenuation cannot be deduced from this transect.

Cyanide. The spatial distribution of cyanide shows the largest gradient of all the parameters, dropping from 2.95 mg/L (HW-01) to non-detectable levels at 200 m. The concentration at 15 m is beyond the WHO/NSDWQ guideline concentration of 0.05 mg/L and is considered an acute toxicological hazard. The estimated half-distance for attenuation of ~44 m is one order of magnitude lower than for organic parameters, mainly because of (i) volatilization of HCN (pKa = 9.2, >99% is volatile at pH < 7), (ii) microbial assimilation by cyanide-tolerant bacterial communities (e.g. Pseudomonas, Bacillus), and (iii) complexation/sorption to metal oxides and organic matter in the vadose zone. The significant drop of 97% in the geochemical zone of 45 m to 120 m is of importance, indicating a critical transition area where cyanide is efficiently removed with the presence of organic loading, and thus makes it as a useful diagnostic contaminant for cassava contamination

Table 3: T*race Metals and Physicochemical Parameters in Hand-Dug Wells Near Cassava Processing Effluent Discharge*

Well ID	Fe (mg/L)	Mn (mg/L)	Zn (mg/L)	Total Hardness (mg/L)	Alkalinity (mg/L)	NO_3^- (mg/L)
HW-01	2.85	1.25	4.10	151	46	18.5
HW-02	1.85	0.95	3.64	130	56	24.2
HW-03	1.62	0.48	1.68	90	67	12.8
HW-04	0.38	0.22	0.18	72	81	8.5
HW-05 Control	0.1	0.12	0.10	68	95	6.2
WHO Limit	0.3	0.4	3	500	-	50
NSDWQ Limit	0.3	0.2	3	150	100	50

The evidence of the redox-driven secondary contamination is given in Table 3. The concentrations of iron (2.85 mg/L) and manganese (1.25 mg/L) at HW-01 are much higher than both the WHO guideline

values (Fe: 0.3 mg/L; Mn: 0.4 mg/L) and the NSDWQ standard (Mn: 0.2 mg/L). The above elevations are not found to be primary contaminants in cassava effluent but are rather the reductive dissolution of Fe(III) and Mn(IV) oxyhydroxides under highly anaerobic conditions caused by decomposition of high concentrations of organic matter. The redox cascade is a secondary process that has been well documented in the infiltration of organic rich effluents in tropical aquifers.

The distance dependent attenuation of Fe and Mn (HW-05: Fe = 0.10 mg/L; Mn = 0.12 mg/L) is consistent with the reduction in organic loading and indicates an increasing lack of reducing conditions away from the source. However, Zn exceeds the stated guideline at HW-01 but is within the limit at the other wells, while nitrate remains within the stated limit. and NO_3^- are within limits in all wells, suggesting that the contamination signature is confined to the cassava-processing stream and does not represent general anthropogenic nitrate loading (such as from agricultural fertiliser). There are inverse distance relationships between the total hardness and the alkalinity, with higher values in close proximity to the source indicating greater mineral weathering under organic rich, acid conditions.

Water Quality Index (WQI) Results

The WQI was computed using 14 parameters with assigned weights based on relative importance. The results are presented in Table 4.

Table 4: Water Quality Index Results and Classification

Well ID	Distance from Mill (m)	WQI	Classification	Drop from HW-01
HW-01	15	96.8	Very Poor	-
HW-02	45	86.42	Very Poor	−10.7 %
HW-03	120	63.35	Poor	−34.6 %
HW-04	200	58.73	Poor	−39.3 %
HW-05 Control	350	47.11	Good	−51.3 %

The WQI decreases from 96.80 at HW-01 to 47.11 at HW-05 indicating gradual improvement in the groundwater-quality classification with increase in distance from the processing area.
The largest single improvement is between 45 m and 120 m (WQI drops 23.07 points) showing that the densest part of the contamination plume is within the first ~100 m.
HW-01 (15 m, WQI 96.8): At the upper limit of “Very Poor.” This is effectively nonpotable without significant treatment.
HW-02 (45 m, WQI 86.42) Still hits hard. It is still in the "Very Poor" class, despite being 3× farther than HW-01. This confirms a powerful point source.
HW-03 & HW-04 (120 – 200 m, WQI 63.35 - 58.73) : Moderate recovery. Both fall within the “Poor” range (51–75), indicating attenuation is active but incomplete.
HW-05 Control (350 m, WQI 47.11): This is the important amendment. The water has crossed the boundary into “Good” quality (WQI < 50) at 350 m. It’s borderline. Only 2.89 points from the 50 limit. But certainly not “Poor”.
The use of HW-05 enhances the Good WQI classification at 350 m from the processing area. The value of 47.11 indicates that while the acute impact of the mill has diminished, the baseline WQI is probably sustained in the 40–50 range due to background geogenic factors (e.g. natural mineralisation, iron, hardness). The data confirm the mill to be the main point source and document effective natural attenuation (dilution, adsorption, filtration) over 350 m. This recovery is evidenced by the reduction in WQI of 51.3 % between 15 m and 350 m.

Geochemistry and Hydrochemical Facies

Major ion concentrations and Piper diagram percentages are presented in Tables 5 and 6.

Table 5: Major Ion Concentrations (mg/L)

Well ID	Ca^{2+} (mg/L)	Mg^{2+} (mg/L)	Na^{+} (mg/L)	K^{+} (mg/L)	HCO_3^{-} (mg/L)	Cl^{-} (mg/L)	SO_4^{2-} (mg/L)	NO_3^{-} (mg/L)
HW-01	50	28.5	85.2	15.8	185	120	85	18.5
HW-02	42.5	25.8	68.5	15.5	155	95	72	24.2
HW-03	38.9	16.5	45.2	12.2	115	88	45	12.8
HW-04	18.5	15.2	28.5	5.5	75	42	28	8.5
HW-05	17.6	7.5	18.2	4.6	52	50	18	6.2
WHO Limit	75	50	200	–	–	250	250	50
NSDWQ Limit	75	50	200	–	–	250	100	50

Table 5 shows the ionic architecture of the polluted groundwater. The most dominant cation in the budget is Na^{+} (85.2 mg/L at HW-01 dropping to 18.2 mg/L at HW-05), closely followed by Ca2+ and Mg2+. For anions, Cl^{-} (120 to 50 mg/L) and HCO_3^{-} (185 to 52 mg/L) are predominant. Strong distance-dependent attenuations are observed for all major ions and are an indication of dilution being a major attenuation mechanism.

In particular, the levels of Cl^{-} and SO_4^{2-} have been raised near the mill. Chloride is not a dominant component of raw cassava tuber, but is added during processing (washing, fermentation brines) and is a conservative tracer of anthropogenic input. This high SO_4^{2-} concentration (85 mg/L at HW-01) may be due to the oxidation of organic sulphur compounds in the effluent and/or the oxidation of sulphide due to the acidic conditions. The progressive decrease in both the ionic concentrations in HW-01 to HW-05 shows that the geophysical low-resistivity anomalies represent actual chemical contamination rather than lithological variations such as clay lenses.

Table 6: Piper Diagram Percentages and Ion Balance

Well ID	Ca%	Mg%	Na+K%	HCO_3%	Cl%	SO_4+NO_3%	T.Cat. (meq/L)	T.An. (meq/L)	CBE%
HW-01	**27.9**	**26.2**	**45.9**	**35.7**	**39.9**	**24.4**	8.95	8.49	**2.66**
HW-02	**27.8**	**27.9**	**44.3**	**35.7**	**37.7**	**26.6**	7.62	7.11	**3.46**
HW-03	**34.8**	**24.3**	**40.9**	**34.2**	**45.0**	**20.8**	5.58	5.51	**0.59**
HW-04	**26.0**	**35.2**	**38.8**	**39.2**	**37.8**	**23.0**	3.55	3.13	**6.28**
HW-05	**36.5**	**25.7**	**37.8**	**31.1**	**51.5**	**17.4**	2.40	2.74	**−6.48**

The major ion data has been converted to a hydrochemical facies using Table 6. The cation triangle shows that Ca and Mg together account for approximately 49.1–61.2% of the total cations, while Na+K contributes approximately 37.8–45.9%. Among the anions, HCO_3^{-} and Cl^{-} are the dominant components, contributing approximately 31.1–39.2% and 37.7–51.5%, respectively, while SO_4^{2-}+NO_3^{-} contributes approximately 17.4–26.6%.

The Piper diagram indicates a mixed hydrochemical facies Ca–Mg–Na–Cl–HCO3 suggesting a combined contribution of alkaline earth and alkali cations and the co-dominance of chloride and bicarbonate among the anions.
The relatively higher Na+K contribution at HW-01 and HW-02 along with their higher chloride concentrations suggest a greater impact of the processing area on the ionic composition of these wells. However, the Piper facies alone does not uniquely identify the source of the dissolved constituents.

The calculated charge-balance errors range from about -6.48 % to +6.28 %. Three samples are within the usual criterion of ±5% with HW-04 and HW-05 slightly higher in imbalance. Therefore, these deviations should be taken into account when interpreting the major-ion facies. The Piper diagram is mainly used to characterise the hydrochemical composition, it does not in itself uniquely identify the source of contamination as cassava effluent

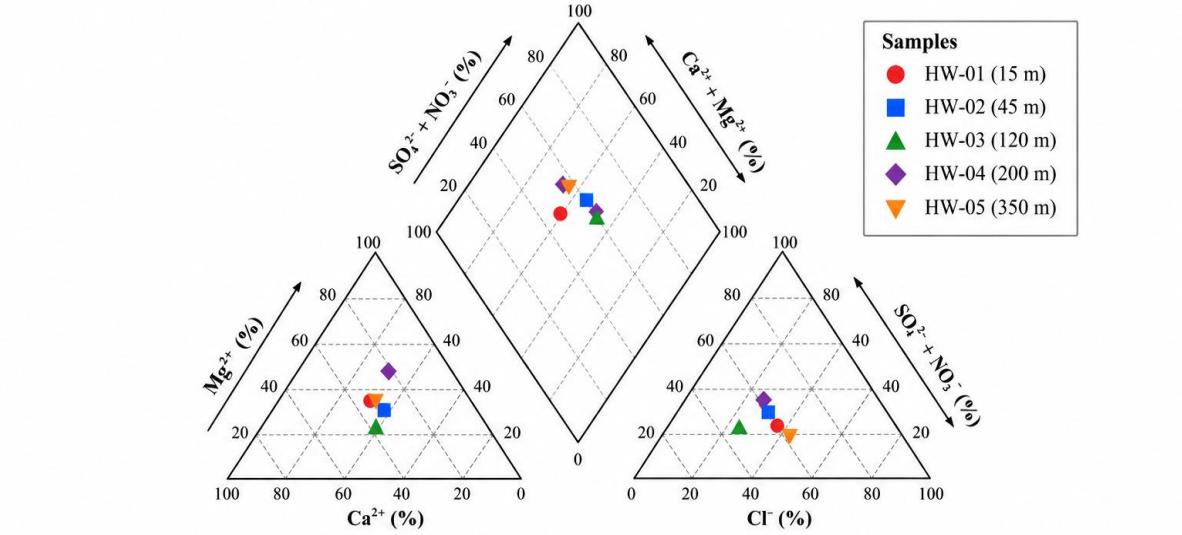


Table 5: Major-ion concentrations of groundwater samples (mg/L)

Parameter	HW-01	HW-02	HW-03	HW-04	HW-05
Ca^{2+}	50	42.5	38.9	18.5	17.6
Mg^{2+}	28.5	25.8	16.5	15.2	7.5
Na^+	85.2	68.5	45.2	28.5	18.2
K^+	15.8	15.5	12.2	5.5	4.6
HCO_3^-	185	155	115	75	52
Cl^-	120	95	88	42	50
SO_4^{2-}	85	72	45	28	18
NO_3^-	18.5	24.2	12.8	8.5	6.2

Table 6: Piper plot parameters and charge balance for groundwater samples

Well ID	Cations (%)			Anions (%)			Total (meq/L)		CBE (%)
	Ca	Mg	Na + K	HCO_3	Cl	$SO_3 + NO_3$	ΣC	ΣA	
HW-01	27.9	26.2	45.9	35.7	39.9	24.4	8.95	8.49	2.66
HW-02	27.8	27.9	44.3	35.7	37.7	26.6	7.62	7.11	3.46
HW-03	34.8	24.3	40.9	34.2	45.0	20.8	5.58	5.51	0.59
HW-04	26.0	35.2	38.8	39.2	37.8	23.0	3.55	3.13	6.28
HW-05	36.5	25.7	37.8	31.1	51.5	17.4	2.40	2.74	-6.48

Figure 4: Piper Diagram and Major Ion Chemistry of Groundwater from Five Monitoring Wells (HW-01 to HW-05) with Water Type Classification

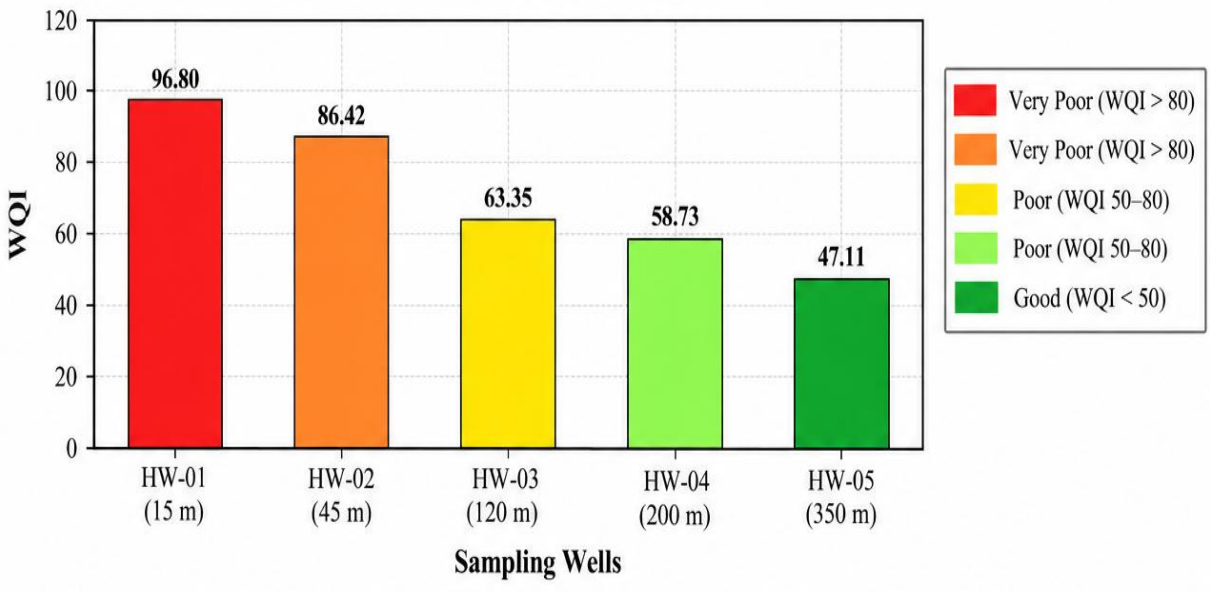


Figure 5 : Water Quality Index variation with Distance from cassava Processing Mill Hand dug wells in the Study Area

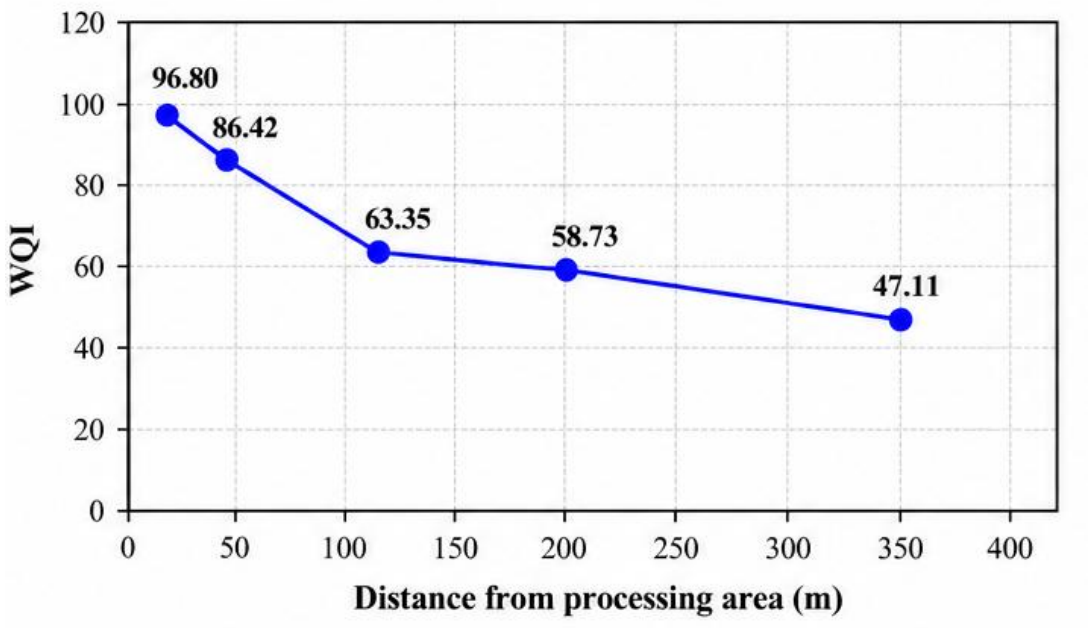


Figure 6 : WQI vs Distance from Cassava Processing Mill

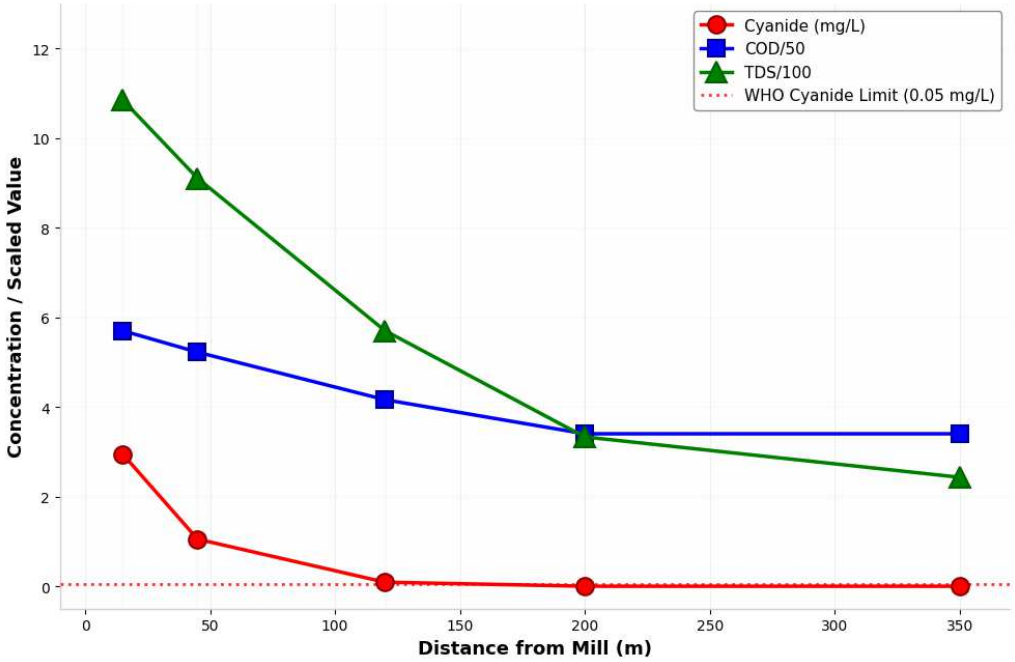


Figure 7: Pollutant Decay With Distance

5.0 Discussion

Integration of Geophysical and Hydrochemical Evidence

The integration of two-dimensional electrical resistivity tomography (ERT), three-dimensional resistivity visualization, vertical electrical sounding (VES), and hydrochemical data provides complementary evidence for characterizing the subsurface conditions associated with cassava-processing activities at Ugbolu. The ERT results revealed a wide resistivity range of approximately 4.12–11,948 Ωm, with several low-resistivity anomalies predominantly occurring within the 10–50 Ωm range. These conductive zones occur from shallow depths of approximately 1.6 m and locally extend to the maximum investigated depth of about 15.9 m. The distribution of these anomalies within the shallow sandy subsurface provides evidence of zones characterized by relatively conductive subsurface conditions.

Low resistivity needs to be interpreted in the geological and hydrochemical setting, since electrical resistivity is driven by the pore fluid conductivity, degree of saturation, porosity, clay content and lithological variation. Consequently, a low-resistivity anomaly alone cannot be used to prove the presence of a specific contaminant. However, in this study, ERT results are accompanied by hydrochemical evidence of degraded groundwater quality such as low pH, high EC and TDS, increased turbidity, elevated organic loading indicators, cyanide, iron and manganese. The coincidence of these independent observations supports the interpretation that

a substantial proportion of the conductive zones is associated with altered groundwater conditions related to the cassava processing environment.

This integrated interpretation is consistent with previous investigations of cassava-processing environments in Nigeria. Adigun and Olorunfemi (2017) demonstrated the value of combining geophysical and hydrochemical investigations around cassava-processing factories in Ilesha. Osinowo et al. (2020) similarly used integrated geophysical methods to delineate conductive zones associated with cassava-effluent leachate, while Ehilenboadiaye et al. (2018) applied 2-D and 3-D resistivity imaging to investigate a contaminant plume associated with a cassava-processing mill in Edo State. More recently, Akinlabi and Akinlade (2024) combined geoelectrical and physicochemical investigations to characterize groundwater contamination around a cassava-processing factory. These studies provide a regional basis for interpreting the convergence between the geophysical and hydrochemical observations at Ugbolu.

The present results therefore support a multi-parameter interpretation in which the resistivity anomalies represent conductive subsurface zones whose significance is constrained by the independently measured groundwater chemistry. This approach is preferable to interpreting the 10–50 Ωm range as a universal contamination threshold because resistivity values are inherently dependent on local geological and hydrochemical conditions (Revil et al., 2012; Martinho, 2023).

Spatial Distribution and Geometry of the Conductive Anomalies

The ERT results show that the conductive anomalies are spatially heterogeneous, and not a single uniform subsurface body. Profile 1 shows a large low-resistivity zone of approximately 10–45 Ωm to a depth of about 15.9 m. The resistivity of Profile 2 is between about 4.12 and 40.2 Ωm and that of Profile 3 between about 7.32 and 37.6 Ωm. Profile 4 has a wider range of 18.9–354 Ωm. Profile 5 shows low resistivity material below about 51Ωm at depth of about 6–8 m. Profile 6 shows conductive zones below about 47.2 Ωm, whereas Profile 7 records about 9.06–62.5 Ωm with conductive material extending to about 10 m. Profile 8 has values lower than about 75.5 Ωm. Profile 9 has a low resistivity zone under about 50 Ωm for part of the profile, while Profile 10 has low resistivity zones under about 52.4 Ωm at both ends of the profile, and a relatively resistive central feature.

The difference in the geometry of the anomalies indicates a nonuniformity of conductive subsurface conditions in space. Anomalies may be laterally extensive or localised. This spatial variability is consistent with heterogeneous distribution of sandy and finer grained materials in shallow subsurface. The electrical current distribution in resistivity imaging is also affected by changes in moisture content, pore water conductivity and lithological composition. Therefore the observed irregular geometry is a representation of the variations in the electrical properties of the subsurface rather than a measured contaminant concentration.

The three dimensional resistivity visualisation (interpolated) further illustrates the spatial variability of the conductive zones. The model shows resistivity values ranging from approximately 20 to greater than 6,000 Ωm, with irregular low-resistivity zones occurring

mainly in the shallow subsurface. The strongest conductive features are found within about the upper 0-10 m. The Quasi-3-D resistivity visualizationrepresentation, therefore, provides a spatial synthesis of the 2-D resistivity sections and shows that the conductive zones have variable lateral and vertical continuity.
The environmental application of ERT to heterogeneous shallow subsurface conditions has been discussed by Dahlin and Loke (1998) and Revil et al. (2012), where the authors pointed out that electrical resistivity distributions are controlled by both geological and pore-fluid properties. The current results also suggest that the geometry of the conductive zones should be interpreted in the geologic context, not as a direct image of the contaminant concentration. The visualisation displays patchy low resistivity zones mainly located in the shallow subsurface, with a general increase in resistivity with distance from the suspected contaminant source.

VES Evidence and Vertical Control of the ERT Interpretation

The ten VES stations give complementary vertical information on the geoelectrical structure of the study area. The interpreted models consist of five geoelectric layers. The resistivities of layer 1 ranged from 14.2 to 413 Ωm, layer 2 ranged between 20 to 441 Ωm, layer 3 ranged between 12.5 to 714 Ωm, layer 4 ranged between 47.9 to 1,626 Ωm, and layer 5 ranged between 127 to 791 Ωm. The large difference in the resistivity values for the layers indicates a heterogeneous electrical character of the shallow subsurface.
The low resistivity values obtained in shallow and intermediate layers give vertical support to the conductive conditions detected by ERT. Conversely, the much higher resistivity values in Layer 5 correspond to the deeper coarse-sand unit that was interpreted in the original results as the main aquifer for fresh groundwater. Therefore, the VES models indicate a change from relatively variable and locally conductive shallow/intermediate materials to a generally more resistive deeper unit.
The resistivity structure from the ERT is consistent with the vertical resistivity structure from the VES. This is important because ERT provides mainly lateral and vertical imaging along profiles while VES provides a one-dimensional picture of the vertical resistivity structure at particular points. The complementarity of these approaches has been demonstrated in the geophysical investigation of heterogeneous near surface environments (Aizebeokhai et al., 2010).
The VES data revealed variable five layer geoelectric sequences, the curve types include HKA, AHA, HA, HK, HAH and KA. The variation shows that the subsurface is not uniform in vertical geoelectric sequence in the study area. Thus, the interpreted layer resistivities and thicknesses provide important vertical constraints on the distribution of conductive and resistive materials associated with the groundwater system and possible contaminant migration.

Hydrochemical Evidence of Groundwater Quality Deterioration

The hydrochemical results indicate a distinct spatial variation among the five sampled wells. HW-01 situated 15 m from processing area recorded highest turbidity 45.2 NTU, highest TDS 1,085 mg/L, highest EC 1,350 µS/cm and lowest pH 4.9. HW-02 located at a distance of 45 m has pH 5.2, EC 1,220 µS/cm, TDS 910 mg/L and turbidity 32.8 NTU. HW-03 located at a

distance of 120 m from the processing area has pH 5.6, EC 890 µS/cm, TDS 570 mg/L and turbidity 18.5 NTU. At HW-04 (200 m away), values are pH 6.5, EC 720 µS/cm, TDS 333 mg/L and turbidity 8.2 NTU. At HW-05 (350 m away), values are pH 6.7, EC 580 µS/cm, TDS 243 mg/L and turbidity 4.5 NTU.

Thus, the measured parameters strongly depend on the distance from the processing area in space. Groundwater from the source is more acidic and has higher EC, TDS and turbidity whereas the more distant wells have progressively higher pH and lower EC, TDS and turbidity. This trend is consistent with more intense hydrochemical alteration in wells nearer to the processing area.

The spatial pattern is similar for several of the major-ion concentrations. Calcium decreases from 50 mg/L at HW-01 to 17.6 mg/L at HW-05, magnesium from 28.5 to 7.5 mg/L, sodium from 85.2 to 18.2 mg/L, potassium from 15.8 to 4.6 mg/L, bicarbonate from 185 to 52 mg/L, chloride from 120 to 50 mg/L and sulphate from 85 to 18 mg/L. Nitrate also dropped from 18.5 to 6.2 mg/L. These changes suggest a systematic spatial change in groundwater chemistry among the sampled locations.

Similar hydrochemical degradation due to cassava processing activities has been reported in other sedimentary environments in Nigeria. Olurin et al., 2022 reported the deterioration of groundwater quality in the vicinity of a cassava-processing mill at Ilaro. Akinlabi and Akinlade, 2024 reported elevated EC, TDS and cyanide associated with groundwater contamination in the vicinity of a cassava-processing facility. The link between these observations and the Ugbolu results provides context to the interpretation of the observed spatial hydrochemical pattern.

Organic Loading: COD and BOD_5

The hydrochemical results are chemical oxygen demand (COD) and biochemical oxygen demand (BOD5) in five days. These parameters give important indications on the organic loading. The concentrations of COD are 285, 261, 208, 170 and 170 mg/L for HW-01 to HW-05 respectively, and BOD5 concentrations are 142, 98, 106, 87 and 74 mg/L respectively. The maximum COD and BOD_5 concentrations are at HW-01, 15 m away from the processing area, and the lowest at HW-05, 350 m away. The spatial distribution indicates a progressive decrease of both the measured indicators of organic load with increasing distance across the sampled wells.

This pattern appears along with changes in spatial distribution of pH, EC, TDS, turbidity and cyanide. The highest values of COD and BOD5 are recorded on HW-01. It also has the highest EC, TDS, turbidity and cyanide concentration and the lowest pH. The COD and BOD5 concentrations measured at HW-05 are significantly lower and the ground water has higher pH and relatively low EC, TDS and Turbidity.

The COD decreases with the distance to the processing area, suggesting a strong spatial attenuation pattern over the sampled wells. Therefore, the spatial relationship between COD and distance is consistent with the observed decrease of COD concentration from the near-source to the distal well.

The highest concentrations were found in the well closest to the cassava processing facility, with decreasing concentrations with increasing distance. The spatial pattern suggests a strong correlation of the cassava-processing area with the observed organic loading in the groundwater.

Cyanide Distribution

Cyanide decreases from 2.95 mg/L at HW-01 to 1.05 mg/L at HW-02, 0.09 mg/L at HW-03 and non-detectable at HW-04 and HW-05.

The distribution shows that the highest measured concentration of cyanide occurs at the location closest to the processing area, and that concentrations decrease with distance from the source. The spatial pattern is consistent with the existence of cyanide in cassava-processing environments and earlier studies that have identified cyanide as a significant hydrochemical indicator in the neighbourhood of cassava-processing facilities (Olurin et al., 2022; Akinlabi & Akinlade, 2024).

The concentration of cyanide decreases progressively with distance from the processing area indicating a strong spatial attenuation pattern. However this decrease may be a result of a combination of dilution, dispersion, transformation and interaction with subsurface material rather than a single controlling process.

The reduction in measured cyanide concentration with distance is not, in itself, proof of the specific process which causes the reduction. Dilution, dispersion, transformation, and interaction with subsurface materials can affect cyanide behaviour in groundwater. Similarly, numerical modelling studies in the Niger Delta have demonstrated the influence of geological and hydrogeological conditions on the transport of cyanide from cassava-processing sources (Ohwoghere-Asuma et al., 2024).

Iron, Manganese and Other Hydrochemical Parameters

The wells closest to the processing area have high levels of iron and manganese. Iron concentrations decrease from 2.85 to 0.10 mg/L, The highest concentrations of both elements are thus observed at HW-01 and the lowest concentrations are observed at HW-05.

High concentrations of Fe and Mn in the groundwater, especially in the wells located close to the cassava processing plant, may be associated with geochemical alterations caused by the organic-rich effluent. Addition of organic matter in the subsurface can stimulate microbial activity and change the geochemical conditions of groundwater, which can lead to the mobilisation of Fe and Mn from aquifer materials [Zhai et al., 2021; Feng et al., 2023]. The general decrease in Fe and Mn concentrations with distance from the processing facility in the present study, along with the associated decrease in organic loading, support a spatial association between effluent influence and Fe/Mn enrichment." Previous studies have reported similar relationships between organic-rich groundwater contamination and Fe/Mn mobilisation [Zhai et al., 2021].

Other hydrochemical parameters also vary systematically between the sampled wells. Zinc decreased from 4.10 to 0.10 mg/L, hardness from 151 to 68 mg/L, alkalinity increased from 46 to 95 mg/L and nitrate decreased from 18.5 to 6.2 mg/L between HW-01 and HW-05. These changes provide further evidence for the spatial variability of groundwater chemistry within the study area .

Hydrochemical Facies and Contaminant Provenance

The Piper analysis indicates a mixed Ca–Mg–Na–Cl–HCO_3 hydrochemical facies. Ca and Mg together account for approximately 49.1–61.2% of the total cations, while Na+K contributes approximately 37.8–45.9%. Among the anions, HCO_3^- and Cl^- are the dominant components, while SO_4^{2-}+NO_3^- contributes a smaller proportion.

The relatively high contribution of Na + K and Cl, particularly in the wells closest to the processing area, indicates that the groundwater chemistry is influenced by processes beyond a simple Ca–Mg-dominated composition. HW-01 and HW-02 show stronger Na–Cl characteristics, indicating a greater contribution of Na and Cl to the groundwater ionic composition at the nearer sampling locations.The major-ion pattern therefore indicates a mixed hydrochemical system in which natural water–rock interaction and anthropogenic influences may both contribute to groundwater composition.

Piper facies alone, however, cannot uniquely identify cassava effluent as the contaminant source because similar Na–Cl or mixed facies can result from several hydrochemical processes. At Ugbolu, the interpretation of anthropogenic influence is strengthened by the simultaneous occurrence of the hydrochemical facies with acidic pH, elevated EC and TDS, organic loading, cyanide, Fe and Mn, and the conductive ERT anomalies.

The calculated errors of charge balance are from about -6.48% to +6.28%. Three samples fall within the commonly applied 5% criterion, while HW-04 and HW-05 show a slightly higher imbalance. These deviations should be considered in the interpretation of the major-ion facies.

Water Quality Index and Groundwater-Quality Pattern

The WQI values decrease from 96.80 at HW-01 to 47.11 at HW-05, indicating progressive improvement in groundwater quality with increasing distance from the processing area. The gradual increase of the WQI with distance from the processing area shows the improving quality of groundwater away from the suspected effluent source. Since the WQI is a composite measure of several water-quality parameters, it is better to interpret it in conjunction with the hydrochemical variables. In this study, the WQI pattern occurs alongside systematic variations in pH, EC, TDS, turbidity, COD, BOD_5, cyanide, Fe, Mn and the major ions.

Comparison with Previous Studies

The Ugbolu results are broadly consistent with previous investigations of cassava-processing contamination in Nigeria. Adigun and Olorunfemi (2017) demonstrated the effectiveness of combining geophysical and hydrochemical measurements around cassava-processing factories at Ilesha. Their integrated approach is particularly relevant to the present study because both investigations use electrical resistivity information together with groundwater chemistry to characterize contamination.

Osinowo et al. (2020) used integrated geophysical techniques to map cassava-effluent leachate contamination at Ilero, while Ehilenboadiaye et al. (2018) investigated contaminant plumes associated with cassava processing using 2-D and 3-D resistivity imaging in Edo State. The occurrence of low-resistivity zones in the Ugbolu study is therefore consistent with the use of electrical resistivity methods for delineating conductive subsurface zones associated with cassava-processing environments.

The hydrochemical observations are also comparable with those of Olurin et al. (2022), who reported groundwater-quality deterioration around a cassava-processing mill in Ilaro, and Akinlabi and Akinlade (2024), who identified relationships between geoelectrical anomalies

and physicochemical indicators of groundwater contamination around a cassava-processing factory in Ogbomoso.

The present study nevertheless differs in its specific combination of ERT, VES, interpolated three-dimensional resistivity visualization and hydrochemical measurements. The concordance between the ERT and VES resistivity structures provides an additional link between the two geophysical data sets and hydrochemical measurements provide the independent information on groundwater quality.

The similarity with previous investigations is thus concerned with the general geophysical and hydrochemical behaviour of cassava-processing environments and not with the fact that the resistivity range or the distribution of contaminants in Ugbolu should be the same as reported in other places.

Integrated Interpretation of the Ugbolu Results

The results collectively point to a consistent relationship between the shallow conductive subsurface and the observed groundwater quality conditions around the cassava-processing area.The ERT investigation revealed numerous low-resistivity anomalies, mainly in the range of 10-50 Ωm, extending from about 1.6 to 15.9 m. VES results independently show significant changes in resistivity at the shallow and intermediate layers and a generally more resistive deeper Layer 5 interpreted as the main freshwater-bearing coarse-sand aquifer.

Hydrochemical data show that the most acidic ground water and the highest measured values of EC, TDS, turbidity, COD, BOD5, cyanide, Fe and Mn concentrations belong to HW-01, located 15 m from the processing area. In general, the farther wells are characterised by lower concentrations of these parameters and higher pH values. The spatial pattern is therefore identified separately in the geophysical and hydrochemical data sets.

The independent geophysical and hydrochemical data sets display consistent spatial patterns. The conductive ERT zones reflect the spatial distribution of the worse quality groundwater and the hydrochemical parameters are generally better with increasing distance from the processing area. The agreement of VES and ERT resistivity structures also supports the interpretation of the subsurface electrical framework.

The combined evidence therefore is consistent with the interpretation of shallow conductive zones as zones of modified subsurface electrical properties spatially coincident with degraded groundwater chemistry. The results do not suggest a single chemical cause for each low-resistivity anomaly, but the convergence of the ERT, VES and hydrochemical observations provides substantially stronger evidence than any single dataset considered independently.

6.0 Conclusion

The study provides combined evidence of groundwater quality deterioration associated with cassava-processing activities at Ugbolu. ERT mapped large low resistivity anomalies in the shallow subsurface.

The vertical succession of the subsurface and aquifer was further studied by the VES. The hydrochemical results confirmed considerable deterioration of groundwater quality in the vicinity of the Processing area. The wells most affected showed high values of COD, BOD 5 , cyanide, Fe and Mn. Indicators of contamination generally decreased with distance from the source of the effluent. The hydrogeochemical facies of the groundwater was mixed Ca-Mg-Na-Cl-HCO3. The hydrochemical evidence was in strong agreement with the geophysical

anomalies.

Such convergence favours spatial association of conductive subsurface zones and degraded conditions of groundwater.
This makes the shallow Benin Formation aquifer highly vulnerable to cassava-effluent contamination. The integration of ERT, VES and hydrochemistry reduced uncertainty in plume delineation. The integrated approach provides a useful framework to evaluate similar groundwater contamination issues.

Acknowledgements
We are very grateful to the Almighty God for his divine guidance and strength throughout the course of this research work.

Author contributions
All authors contributed to the design and concept of the study. Ighodalo John Elvis and Ikere Povwe Joy drafted the first version. Figures and tables were prepared and interpreted by Alexander Ogbamikhumi. All authors have read and approved the final manuscript.

Financing
There was no money available

Availability of data
All data generated or analysed during this study are included in this published article.

Ethics approval
Not applicable.

Consent for publication
N/A

Consent for publication Not applicable.
N/A

Competing interests
The authors declare that there are no competing interests.

REFERENCES

Adigun, E. O., & Olorunfemi, M. O. (2017). Integrated geophysical and hydrochemical investigations of subsoil and groundwater pollution around three cassava processing factories at Ireti-Ayo community, Ilesha, Southwestern Nigeria. *Ife Journal of Science, 19*(2), 255–264. https://doi.org/10.4314/ijs.v19i2.6

Aizebeokhai, A. P., Olayinka, A. I., & Singh, V. S. (2010). Application of 2D and 3D geoelectrical resistivity imaging for engineering site investigation in a crystalline basement terrain, southwestern

Nigeria. *Environmental Earth Sciences, 61*, 1481–1492. https://doi.org/10.1007/s12665-010-0464-z

Akinlabi, I. A., & Akinlade, Z. A. (2024). Geoelectrical and physicochemical characterization of groundwater contamination around a cassava processing factory in Ogbomoso, Southwestern Nigeria. *International Journal of Environment and Climate Change, 14*(6), 13–23. https://doi.org/10.9734/ijecc/2024/v14i64207

Alile, O. M., Aigbogun, C. O., Enoma, N., Abraham, E. M., & Ighodalo, J. E. (2017b). 2D and 3D electrical resistivity tomography (ERT) investigation of mineral deposits in Amahor, Edo State, Nigeria. *Nigerian Research Journal of Engineering and Environmental Sciences, 2*(1), 215–231.

Alile, O. M., Ighodalo, J. E., & Aigbogun, C. O. (2017a). Application of 3D electrical resistivity tomography for geoenvironmental investigation at Otofure, Edo State, Nigeria. *SEG International Exposition and Annual Meeting*, SEG-2017-17726998.

Amidu, S. A., & Olayinka, A. I. (2006). Environmental assessment of sewage disposal systems using 2-D Electrical Resistivity Tomography and geochemical analysis: A case study of Ibadan, Southwestern Nigeria. *Environmental and Engineering Geoscience, 12*, 261–272.

APHA (2017). *Standard Methods for the Examination of Water and Wastewater*, 23rd Edition. American Public Health Association, Washington, DC.

Awomeso, J. A., Taiwo, A. M., Gbadebo, A. M., & Adenowo, J. A. (2010). Pollution of water body by textile industry effluents in Lagos, Nigeria. *Journal of Applied Sciences in Environmental Sanitation, 5*(4), 353–359.

Brown, R. M., McClelland, N. I., Deininger, R. A., & Tozer, R. G. (1972). A water quality index—crashing the psychological barrier. *Proceedings of the Annual Conference of the American Water Works Association, 1*, 13–18.

Cosenza, P., Marmet, E., Rejiba, F., Cui, Y. J., Tabbagh, A., & Charlery, Y. (2006). Correlations between geotechnical and electrical data: A case study at Garchy in France. *Journal of Applied Geophysics, 60*(3–4), 165–178. https://doi.org/10.1016/j.jappgeo.2006.02.003

Dahlin, T., & Loke, M. H. (1998). Resolution of 2D Wenner resistivity imaging as assessed by numerical modelling. *Journal of Applied Geophysics, 38*(4), 237–249. https://doi.org/10.1016/S0926-9851(97)00030-X

Ehilenboadiaye, J. I., Aigbogun, C. O., & Osamudiamen, G. (2018). 2D and 3D subsurface geo-electrical resistivity imaging of contaminant plume from cassava processing mill in Uzebba Area of Edo North, Edo State, Nigeria. *Journal of Applied Sciences and Environmental Management, 22*(4), 539–543. https://doi.org/10.4314/jasem.v22i4.17

Ekpechi, O. L. (1994). Cassava cyanogenesis and iodine deficiency disorders—cassava safety. *Acta Horticulturae, 375*, 289–292.

Emagbetere, J. U., Jegede, S. I., & Ighodalo, J. E. (2018). Application of two geophysical methods to characterize cassava effluents at selected processing mills at Owan West, Edo State, Nigeria. *Journal of the Nigerian Association of Mathematical Physics, 45*(1).

Feng, F., Jiang, Y., Jia, Y., Shang, C., Lian, X., Zang, Y., & Zhao, M. (2023). Risks of nutrients and metal(loid)s mobilization triggered by groundwater recharge containing reactive organic matter. *Journal of Hydrology, 623*, 129780. https://doi.org/10.1016/j.jhydrol.2023.129780

Federal Republic of Nigeria. (2002). *National Water Supply and Sanitation Policy* (1st ed.). Federal Ministry of Water Resources, Abuja, Nigeria, pp. 7–11.

Forster, C. F., Quek, S. Y., & Wase, D. A. J. (1998). The use of sago waste for the sorption of Pb and Cu. *Water SA, 4*(3), 251.

Ighodalo, J. E., & Airen, O. J. (2024). Application of 2D and 3D geoelectrical imaging for site investigation at a proposed hotel building site in Benin. *Journal of Energy Technology and Environment, 6*(2), 250–259.

Ighodalo, J. E., & Japhet, O. J. (2024). Delineation of aquiferous formation using 2-D electrical imaging technique at Ukwuani, South–South Nigeria. *Journal of Energy Technology and Environment, 6*(2), 46–54.

Ighodalo, J. E., & Ohioma, J. O. (2024). Application of quasi-3D electrical resistivity imaging techniques to site investigations in Mosogar, Ethiope West LGA, South-South Nigeria. *Transactions of the Nigerian Association of Mathematical Physics, 20*(1), 23–30.

Ighodalo, J. E., & Okanigbuan, P. N. (2022). Delineation of leachate plume migration using geo-electrical resistivity on Otofure Dumpsite in Benin-City, Nigeria. *Transactions of the Nigerian Association of Mathematical Physics, 18*, 55–62.

Iyoha, A., Ighodalo, J. E., & Okanigbuan, P. N. (2020). Geophysical investigation of leachate plume in waste disposal site: A case study of Otofure Dumpsite, Ovia North-East Local Government Area of Edo State, Nigeria, using 3D Electrical Resistivity Tomography. *BIU Journal of Basic and Applied Sciences, 5*(1), 15–26.

Itsueli, D., Ogbamikhumi, A., and Ossai, F. (2026). Sustainable Groundwater Appraisal of the Lignite Series at Irrua Esan Central Local Government Area Edo State Nigeria. Journal of Applied Science and Environmental Management 30(9B), 3286-3294.

Loke, M. H. (2010). *RES2DINV ver. 3.59: Rapid 2-D resistivity and IP inversion using the least-squares method (User manual).* Geotomo Software.

Martinho, E. (2023). Electrical resistivity and induced polarization methods for environmental investigations: An overview. *Water, Air, & Soil Pollution, 234*(4), 215. https://doi.org/10.1007/s11270-023-06214-x

Morris, B. L., Lawrence, A. R. L., Chilton, P. J. C., Adams, B., Calow, R. C., & Klinck, B. A. (2003). *Groundwater and its susceptibility to degradation: A global assessment of the problem and options for management.* United Nations Environment Programme (UNEP).

Ohwoghere-Asuma, O., Chinyem, F. I., Atiti, P., & Ophori, D. (2024). Contaminant transport modelling of the vulnerability of aquifer to cyanide from cassava processing mill in the western Niger Delta. *HydroResearch, 7*, 154–163. https://doi.org/10.1016/j.hydres.2024.02.001

Okunade, D. A., & Adakalu, K. O. (2013). Physico-chemical analysis of contaminated water resources due to cassava wastewater effluent disposal. *European Journal of Science and Technology, 2*(6), 75–78.

Olayinka, A. S. (2013). Assessment of toxic potentials of cassava effluent on *Clarias gariepinus*. *International Agricultural Journal of Science and Research, 3*(3), 157.

Olurin, O. T., Ganiyu, S. A., Ogunsanwo, F. O., Ojo, A. O., Alabi, A. A., & Adegbamigbe, O. K. (2022). Groundwater quality assessments around a cassava processing mill on the sedimentary terrain of Ilaro, South-western Nigeria. *HydroResearch, 5*, 108–117. https://doi.org/10.1016/j.hydres.2022.11.002

Omotioma, M., Mbah, G. O., Akpan, I. J., & Ibezim, O. B. (2013). Impact assessment of cassava effluents on Barika Stream in Ibadan, Nigeria. *International Journal of Environmental Science and Management and Engineering Research, 2*(2), 50–52.

Osinowo, O. O., Agbaje, M. A., & Ariyo, S. O. (2020). Integrated geophysical investigation techniques for mapping cassava effluent leachate contamination plume, at a dumpsite in Ilero, southwestern Nigeria. *Scientific African, 8*, e00374. https://doi.org/10.1016/j.sciaf.2020.e00374

Revil, A., Karaoulis, M., Johnson, T. C., & Kemna, A. (2012). Review: Some low-frequency electrical methods for subsurface characterization and monitoring in hydrogeology. *Hydrogeology Journal, 20*(4), 617–658. https://doi.org/10.1007/s10040-011-0819-x

Reyment, R. A. (1965). *Aspects of the geology of Nigeria.* Ibadan University Press.

Samouëlian, A., Cousin, I., Tabbagh, A., Bruand, A., & Richard, G. (2005). Electrical resistivity survey in soil science: A review. *Soil and Tillage Research, 83*(2), 173–193. https://doi.org/10.1016/j.still.2004.10.004

Salami, S. A., & Ogbamikhumi, A. (2017). Geo-Electrical Investigation for Groundwater Potential of Ihievbe Ogben, Edo North, South Western Nigeria. Journal of Applied Science & Environmental Management, 21(7), 1291-1293.

Short, K. C., & Stauble, A. J. (1967). Outline of geology of Niger Delta. *AAPG Bulletin, 51*(5), 761–779. https://doi.org/10.1306/5D25C0CF-16C1-11D7-8645000102C1865D

World Health Organization (WHO). (2017). *Guidelines for Drinking-water Quality*, 4th Edition incorporating the 1st Addendum. WHO, Geneva.

Zhai, Y., Han, Y., Xia, X., Li, X., Lu, H., Teng, Y., & Wang, J. (2021). Anthropogenic organic pollutants in groundwater increase releases of Fe and Mn from aquifer sediments: Impacts of pollution degree, mineral content, and pH. *Water, 13*(14), 1920. https://doi.org/10.3390/w13141920